Experimental determination of vertical instability strength in PDX tokamak

1982 Nucl. Fusion 22 1597

(http://iopscience.iop.org/0029-5515/22/12/006)

EXPERIMENTAL DETERMINATION OF VERTICAL INSTABILITY STRENGTH IN PDX TOKAMAK

H. TAKAHASHI, K. BOL, H. MAEDA*,
M. OKABAYASHI, M. REUSCH
Plasma Physics Laboratory,
Princeton, New Jersey,
United States of America

ABSTRACT. The instability strength of a diverted plasma with vertical elongation is measured for a range of the magnetic-field decay index, $-1.5 < n < +0.5$, in the standard-D and inverted-D configurations. The range of the instability growth time is from one to four orders of magnitude greater than previously published results. When the plasma current is in the range of 170–310 kA, the instability can be suppressed by passive stabilization due to currents induced in a discrete coil system together with a moderate-power (100 kW) active feedback system. The inverted-D configuration is three times more unstable than the standard-D configuration for the same ellipticity. The inverted-D configuration is destabilized by its negative triangularity and the standard-D is stabilized by its positive triangularity.

1. INTRODUCTION

Elongated plasmas are invariably considered in tokamak reactor designs [1] because of their expected higher beta limit, greater plasma volume for a given q-value, and economical use of the volume within D-shaped toroidal field (TF) coils. Tokamak reactors may also have divertors for heat and particle removal. Use of poloidal divertors may also result in elongated plasmas. When two divertors are employed in a conventional top/bottom divertor configuration, balanced loading of the divertors becomes an important consideration as the heat and particle loading of the divertor plates in large tokamaks approaches the limits set by materials considerations. The so-called single-null configuration, in which only one divertor is used, is also considered for reactors to further economize the toroidal field volume and to eliminate difficulties associated with the simultaneous control of the two null-point locations. Vertically elongated plasmas are, however, often rendered unstable by the same forces that generate the elongation: a slight axisymmetric displacement of the plasma from its equilibrium position will cause it to move unstably upward or downward. Control of the vertical position in the face of this axisymmetric instability is an important requirement for future tokamak reactors. Furthermore, effective vertical position control may possibly enable a novel tokamak design and operational concept [2] i.e. a negative-n-index tokamak with the radial stability substantially better than that of conventional positive-n-value tokamaks. The principal objective of the work reported here is to provide a detailed analysis of vertical instability experimental data to which theoretical predictions can be compared. Theories on the axisymmetric instability and an extensive list of references before 1978 can be found in a review article by Wesson [3].

The vertical instability studied here is in the passively stabilized regime. As the plasma moves, currents are induced in its surrounding structures, generating a stabilizing radial field. The plasma motion takes place only because of resistive decay of the induced currents. This resistive time-scale instability is amenable to stabilization by means of feedback control [4]. In many experimental devices, currents induced in the vessel walls are important in providing the stabilizing radial field. These currents flow in ill-defined patterns and are difficult to measure. In the PDX tokamak [5], the only significant stabilizing currents flow along well-defined paths in the divertor coils and shorting bars. Furthermore, these currents are experimentally measurable. This feature enables determination of the 'equilibrium loop currents' and calculations of the radial field error corrections which are essential to accurate measurements of small instability growth rates. For this reason, the PDX device is well suited

* Japan Atomic Energy Research Institute, Tokai-Mura, Ibaraki-Ken, Japan.

for measurements of instability growth rates and for testing the efficacy of passive stabilization by a discrete coil structure.

There were several experimental studies of the vertical stability of elongated tokamak plasmas. The work in the T-12 tokamak [6] dealt with a situation in which most of the stabilizing effects were provided by thick copper shells. Passive stabilization effects were verified, but few quantitative details were reported on the growth rate or its parametric dependence. Experiments with the TOSCA tokamak [7] were conducted with passive stabilization provided by external windings and vacuum vessel walls. The observed growth time (30–200 μs) is up to thirty times the Alfvén transit time. The data were reported to be in good agreement with theoretical calculations in this regime. Experiments with the Tokapole [8] were in a passively stabilized regime with a time scale of up to one thousand times the Alfvén time. The observed growth time (500 μs) was one order of magnitude smaller than the resistive decay time (~15 ms) of the stabilizing currents induced in the structure. The discrepancy was attributed to large resistance of the low-temperature plasma that had an L/R-time of about 1 ms. The PDX experiments have characteristic times which are several orders of magnitude greater than those of the earlier experiments and simulate more closely situations that might be encountered in fusion reactor environments. The observed growth time is in the range of 0.02–1.0 s (10^4-10^6 times the Alfvén transit time). Slow drift of the plasma at velocities ranging from 0.2 to 1.0 $m \cdot s^{-1}$ is followed over a period of 30–350 ms and over a distance of up to 9 cm to determine the instability growth rate. Although the measured growth time approaches in some cases the plasma L/R-time, no correlation is found in PDX between the two times.

Preliminary experimental results reported earlier [5] are extended to include both the standard-D and inverted-D configurations. In contrast to a conclusion reached in the Tokapole experiments [8], the inverted-D configuration in the PDX is found much more unstable than the standard-D configuration for the same degree of elliptical elongation. Detailed analysis reported here shows that experimental determination of the growth rate is strongly affected by small radial field errors when long growth times are involved. When these errors are properly accounted for, the experimental and theoretical results are in agreement with each other [9]. The experimental growth rate is compared with theoretical predictions based upon progressively more sophisticated physical models. First, the experimental data are presented simply against the major radius locations of the magnetic axis and against the magnetic-field decay index (n-index) at these locations. The experimental growth rate is then compared with prediction of a line current theory and of an analytical theory of Wesson [3] based upon a cylindrical, elliptically elongated plasma surrounded by a confocal resistive wall. A higher-order correction due to a triangular deformation of the plasma is also considered. The relative magnitude of this correction is compared to that of an analytical theory of Yamazaki et al. [10].

In Section 2.1, PDX equilibria are characterized in terms of the n-index and a set of plasma shape parameters. These are obtained by numerical calculations and are used in a later section to derive theoretical growth rates. In Section 2.2, a theory based upon a model in which the plasma is represented by a line current is developed. A notion of equilibrium loop currents is also introduced in this section to formulate a method of correcting for small radial error fields. In Section 3.1, experimental facilities are described. A transfer function technique is outlined in Section 3.2. The technique is used to determine the plasma position and also to compute equilibrium loop currents. The plasma position measurements and experimental procedures used to determine the growth rate are explained in Section 3.3. The correction for radial error fields is discussed in Section 3.4. In Section 3.5, the experimental growth rate is presented as a function of the radial plasma position. In Section 4.1, the experimental growth rate is plotted against the n-index value and is then compared with predictions based upon the line current model. In Section 4.2, comparisons are made between the experimental data and the growth rate as computed from an asymptotic form of Wesson's analytical formula [3]. Corrections for a triangular deformation of the plasma are considered in Section 4.3. Conclusions are drawn in Section 5.

2. THEORY

Analytical theories of the vertical instability often relate the instability strength to one or more of dimensionless parameters which characterize the shape of magnetic surfaces such as the n-index, ellipticity, triangularity and rectangularity. In this section, a systematic way of defining such parameters in terms of a Fourier expansion is described. The simplest form of the instability theory is based upon a representation

of the plasma as a line current. This theory is developed in this section taking the peculiarities of the PDX device into account. A notion of the equilibrium loop currents is also introduced in the process. The equilibrium loop currents determined using a transfer function technique are a useful means of correcting for time-varying radial error fields. Such corrections become increasingly important as the growth time becomes large and the eddy currents induced by plasma motion become comparable to currents induced by external sources. The simple version of this theory is also used to investigate effects of a finite plasma resistivity on the vertical instability strength.

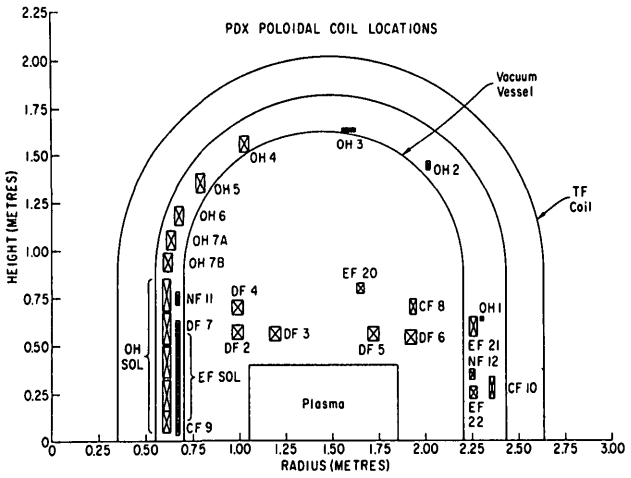

FIG. 1. Cross-sectional view of PDX device showing locations of poloidal-field coils. Only upper half-plane is shown. Coil system is nominally symmetric with respect to structural meridian plane with the exception of toroidal field busswork (not shown).

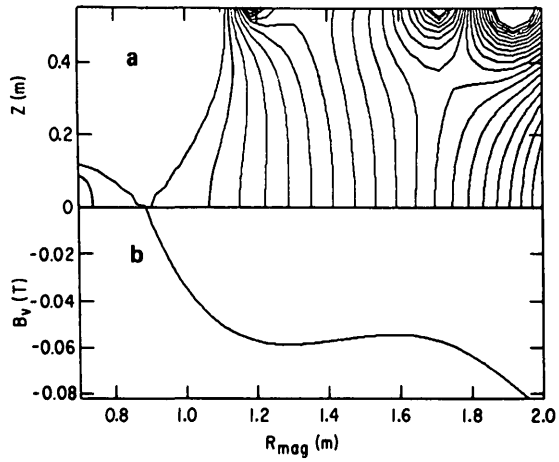

FIG. 2. (a) Vacuum poloidal flux pattern in R–z plane (upper half-plane only); (b) vertical magnetic field variation along meridian plane for diverted PDX plasma. Plasma current goes into page and equilibrium vertical field points downward.

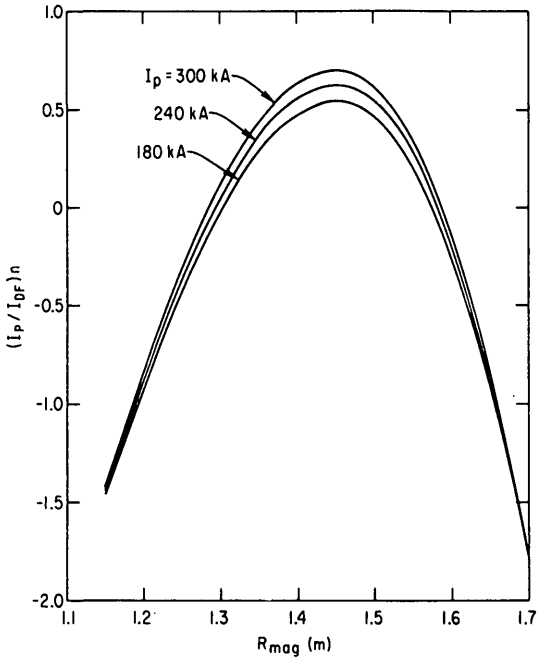

FIG. 3. Vertical magnetic-field decay index (n-index) as a function of magnetic axis location for three different plasma currents, I_p = 180, 240 and 300 kA, and for one DF current, I_{DF} = 11.5 kA. Ordinate is decay index times (I_p/I_{DF}), where I_p is in units of 240 kA and I_{DF} in units of 11.5 kA.

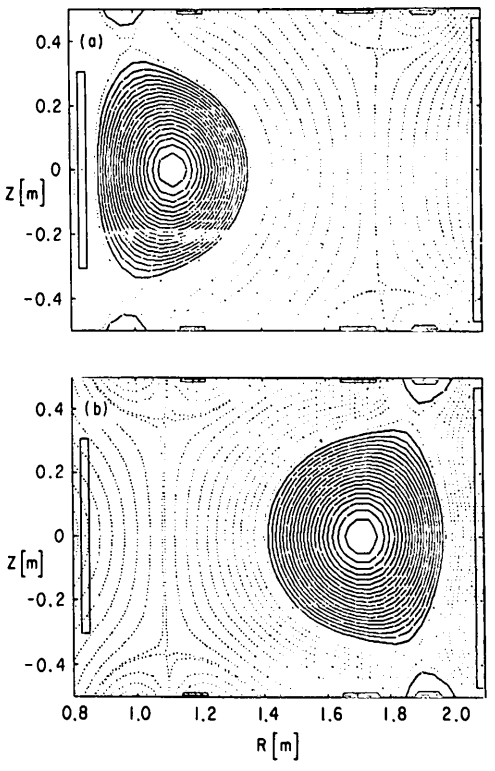

FIG. 4. Poloidal flux surface patterns in (a) inner and (b) outer unstable regions.

2.1. Equilibria in PDX

A cross-sectional view of the PDX device is shown in Fig. 1, indicating the locations of poloidal-field coils. An example of the vacuum poloidal flux pattern is shown in Fig. 2a. R and z in this figure are the major radial and vertical co-ordinates, respectively. Only the upper half plane is shown. The sign of the plasma current is taken to be positive [into the page in Fig. 2a] and the vertical equilibrium field (EF) is therefore negative (downward). Variation of the EF field with the major radius along the structural meridian plane is also shown in Fig. 2b. The equilibrium distribution of the plasma current is computed by using a modified version of the PEST code [11]. This is a free-boundary, toroidally symmetric, ideal-MHD, two-dimensional equilibrium code. For given magnetic axis location, plasma (I_p) and divertor field coil currents (I_{DF}), the required EF current and resultant plasma flux surfaces are obtained. From these poloidal-field (PF) coil currents, the magnetic-field decay index (n-index), $-(R/B_v)\partial B_v/\partial R$, where B_v is the vertical magnetic field, is computed at the magnetic axis location. The variation of the n-index obtained this way as the magnetic axis is moved is shown in Fig.3 for three different values of the plasma current, I_p = 180, 240 and 300 kA, and for the same value of the divertor field (DF) current, I_{DF} = 11.5 kA. The ordinate of the graph is the n-index multiplied by the ratio, I_p/I_{DF}, where I_p is in units of 240 kA and I_{DF} in units of 11.5 kA. Both the small-major-radius region ($R < 1.3$) and the large-major-radius region ($1.6 < R$), over which the n-index is negative, are regions of vertical instability. The vacuum poloidal flux pattern in unstable regions is convex toward the symmetry axis of the device (see Fig. 2). These regions will be referred to as the inner and outer unstable regions, respectively. The central region ($1.3 < R < 1.6$) is the stable region. The plasma is maintained in the stable region during routine operation of PDX.

An example of the poloidal flux surfaces in the presence of a plasma is shown in Fig. 4 for each of the unstable regions. The outermost flux surface is represented by the following Fourier series:

$$r(\theta) = \sum_{n=0}^{\infty} \tilde{a}_n \cos n\theta \qquad (1)$$

where r is the minor radial co-ordinate and θ the minor azimuthal co-ordinate about the point $R = R_G$ and

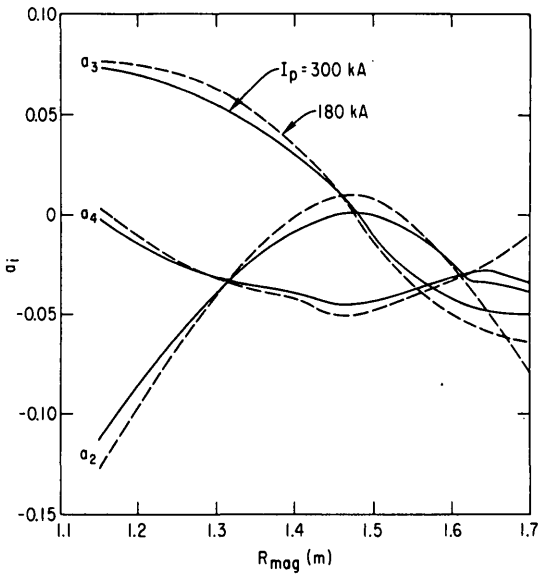

FIG. 5. Fourier expansion coefficients of outermost magnetic-flux surface as functions of magnetic-axis location. a_2 is ellipticity, a_3 triangularity, a_4 rectangularity. Note that triangularity has opposite signs in inner and outer unstable regions. Coil currents used are I_{TF} = 30 kA, I_{DF} = 11.5 kA, $I_{OH} = I_{NF}$ = 0 kA; I_{EF} varies for different major radial locations.

z = 0, in the (R, z) plane. The coefficients of the series and R_G are determined by requiring that the difference between the surface represented by this expression and the actual surface be minimized in the least-square sense and that the coefficient, $\tilde{a}_1$, which represents, to lowest order, a simple horizontal translation of the plasma, be zero. The major radial location, R_G, of the origin of the (r, θ) co-ordinate system chosen in this way is referred to as the geometrical axis of the plasma. $\tilde{a}_0$ is a measure of the plasma minor radius. The normalized coefficients, $a_n = \tilde{a}_n/\tilde{a}_0$, characterize the deviation of the plasma shape from a circle. In particular, a_2 is a measure of the ellipticity, a_3 of the triangularity, and a_4 of the rectangularity. It should be noted that the definitions of these shape parameters used here are related to but not same as parameters defined by Rebhan and Salat [12]. Variations of these normalized shape parameters, a_2 through a_4, are shown in Fig.5 as functions of the magnetic-axis location. A negative value of the ellipticity signifies vertical elongation. A positive triangularity is obtained in the inner unstable region resulting in a standard-D configuration, and a negative triangularity is for the outer unstable region with an inverted-D configuration.

These parameters vary little with the plasma current, except near the largest major radius end where the plasma with a large current begins to come into contact with a limiter.

2.2. Stability theory based upon line plasma current

A simple stability theory is presented in this section based upon a filamentary plasma carrying a constant current. In spite of its simplicity, the model takes into account both the basic cause of instability, i.e. competing attractive forces from the top and bottom divertor currents, and the basic stabilizing effect, e.g. currents induced in coils and structures that produce a stabilizing radial magnetic field. Incompleteness of the model arises primarily from the fact that both the cause and the effect are evaluated at a single spatial point while an actual plasma occupies a finite volume. Nevertheless, the line current theory serves as a good intermediary between experiments and theory because it is easily calculable.

The poloidal field in PDX is generated primarily by a set of four poloidal-field (PF) coil groups; Ohmic heating (OH), equilibrium field (EF), divertor field (DF) and null-field (NF) groups. A part of the toroidal-field (TF) coil group consisting of the turn-to-turn transitions, coil-to-coil transitions and cancellation loop also produces a poloidal field. Currents in these five coil groups are driven by their respective power supplies and will be termed external currents (abbreviated as E-currents). There are also four closed current paths (loop current circuits) within the DF coil group. Currents in these circuits produce a radial field for vertical plasma position control when they are driven by a radial field (RF) amplifier. Loop currents driven through flux linkage with the plasma also generate a stabilizing radial field when the plasma moves vertically under the influence of the instability. These PF coil groups are described in greater detail in Section 3.1 (see also Figs 1 and 6).

The four loop current (L-current) circuit equations can be written in the following matrix form:

$$(\vec{\vec{L}}_{\ell\ell}\dot{\vec{I}}_\ell + \vec{\vec{R}}_{\ell\ell}\vec{I}_\ell) + \frac{d}{dt}(I_p\vec{M}_\ell) + \vec{\vec{L}}_{\ell e}\dot{\vec{I}}_e = \vec{V}_\ell \qquad (2)$$

Here, $\vec{\vec{L}}_{\ell\ell}$ is a 4 X 4 inductance matrix for the L-circuits and $\vec{I}_\ell$ is a four-element one-column (indicated by a right arrow on top of the symbol) array for the L-currents. $\vec{\vec{R}}_{\ell\ell}$ is a diagonal matrix of the L-circuit resistances. $\vec{M}_\ell(R, z)$ is a four-element one-column array for the mutual inductances between the plasma and each of the L-circuits. $\vec{\vec{L}}_{\ell e}$ is a 4 X 5 matrix of the mutual inductances among the four L-circuits and five E-circuits. $\vec{I}_e$ is a five-element one-column array representing the E-currents and $\vec{V}_\ell$ is a four-element one column array for the voltages applied by the RF amplifier. A dot ($\cdot$) indicates differentiation with respect to time. The first two terms of Eq. (2) represent the electromotive force (EMF) due to circuit interactions among the L-circuits. The third term is the EMF generated through flux coupling to a plasma. The fourth term is caused by the time-varying E-currents. The plasma circuit equation is given by

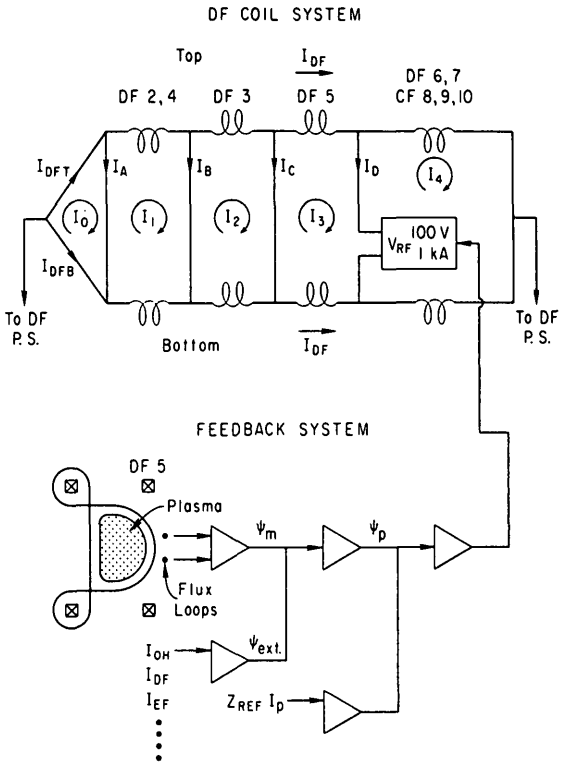

FIG. 6. Equivalent DF/loop current circuits. Vertical-position feedback circuit is also shown schematically.

$$(L_p\dot{I}_p + R_pI_p) + \frac{d}{dt}(\overleftarrow{M}_\ell\vec{I}_\ell) + \frac{d}{dt}(\overleftarrow{M}_e\vec{I}_e) = 0 \qquad (3)$$

where $\vec{M}_e(R, z)$ is a five-element one-column array for the mutual inductances between the plasma and each of the E-circuits. One-row array formed from transposing a one-column array is indicated by a left arrow on top of the symbol.

In the resistive time-scale approximation used here the plasma inertial force is ignored. Vertical force

balance then requires that the radial field at the plasma generated by all sources add up to zero, i.e.

$$\overleftarrow{M}_e' \vec{I}_e + \overleftarrow{M}_\ell' \vec{I}_\ell = 0 \tag{4}$$

where a prime ($'$) represents differentiation with respect to the vertical co-ordinate, z. Radial force balance requires that the hoop force be equal to the force acting on the plasma current due to vertical fields generated by all sources, i.e.

$$\overleftarrow{M}_e^* \vec{I}_e + \overleftarrow{M}_\ell^* \vec{I}_\ell + \frac{\mu_0 I_p}{2} \Lambda = 0 \tag{5}$$

where a star (*) indicates differentiation with respect to the major radial co-ordinate, R. The last term of this equation represents the magnetic flux required for radial equilibrium. The proportionality factor between the required vertical magnetic field, B_{eq}, and the plasma current is designated by

$$\Lambda = -\frac{4\pi R B_{eq}}{\mu_0 I_p} \tag{6}$$

For a pressureless uniform current $\Lambda = \log(8R/a) - 5/4$, and in Shafranov's approximation, $\Lambda = \log(8R/a) - 3/2 + \ell_i/2 + \beta_p$, where a, ℓ_i and β_p are the plasma minor radius, the dimensionless internal inductance and the ratio of the thermal to the poloidal magnetic pressures, respectively.

Equations (2) through (5) are the basic set of equations for the unknowns, $\vec{I}_\ell$, R, z and I_p. In the PDX experiments, the instability growth rate is measured while the plasma current and major radius are held constant. In the following analysis terms involving $\dot{R}$ and $\dot{I}_p$ are ignored, thus making Eqs (3) and (5) redundant. At the end of this section, however, effects of a finite plasma resistivity on the instability strength will be investigated by using a simpler model with only one stabilizing circuit. I_p is then assumed to vary with time.

The loop currents, $\vec{I}_\ell$, are the total currents and consist of two parts: one part is driven by the external power supplies and the other driven by the flux linkage to a moving plasma. The externally driven loop currents determine the equilibrium vertical position of the plasma while the total loop currents determine the actual vertical plasma position. The actual plasma position moves either toward or away from the equilibrium position depending upon whether the equilibrium is stable or unstable, respectively. The rate at which this motion takes place represents the strength of the instability. It must, however, be noted that the externally driven loop currents and hence the equilibrium position may also be changing with time. Under such circumstances the plasma position must be measured with respect to the instantaneous equilibrium position. When a fast instability growth rate is to be measured, this effect of time-varying equilibrium position is often negligible. The effect becomes significant, however, when a slow growth rate with a growth time comparable to the discharge duration is to be determined as is the case in the PDX experiments. The success of the PDX experiments rests, in part, on the fact that the time-varying equilibrium position could be determined experimentally.

The externally driven loop currents (termed equilibrium currents), $\vec{I}_q$, are governed by the equation

$$\vec{\vec{L}}_{\ell\ell} \dot{\vec{I}}_q + \vec{\vec{R}}_{\ell\ell} \vec{I}_q + \vec{\vec{L}}_{\ell e} \dot{\vec{I}}_e = \vec{V}_\ell \tag{7}$$

In a system with a perfect vertical symmetry, coupling between the external and the loop current circuits is absent and all elements of the matrix, $\vec{\vec{L}}_{\ell e}$, are zero. Experimentally, however, small but non-negligible currents are driven by the external power supplies, due to a slight asymmetry of the system. The equilibrium currents are also driven by the RF amplifier when the vertical position feedback control is engaged, i.e. $\vec{V}_\ell \neq 0$. These equilibrium loop currents produce a radial field distribution. The location at which this field is zero is the equilibrium position, (R_q, z_q). It satisfies the equation

$$\overleftarrow{M}_e' \vec{I}_e + \overleftarrow{M}_\ell' \vec{I}_q = 0 \tag{8}$$

A governing equation for the vertical instability is obtained from Eqs (2), (4), (7), and (8) under the condition of constant plasma current and major radius by linearizing these equations and expanding the mutual inductances, $\vec{M}_\ell$ and $\vec{M}_e$, into a Taylor series in z about the equilibrium position, z_q. After straightforward algebraic manipulations, we obtain

$$(\dot{\vec{I}}_\ell - \dot{\vec{I}}_q) + (\vec{\vec{n}} + \vec{\vec{n}}_s)^{-1} \vec{\vec{n}} \vec{\vec{L}}_{\ell\ell}^{-1} \vec{\vec{R}}_\ell (\vec{I}_\ell - \vec{I}_q) = 0 \tag{9}$$

A small term involving a logarithmic time derivative of $\overleftarrow{M}_e''(z_q)\vec{I}_e$ is neglected in arriving at this equation. The fact that $\vec{M}_\ell'$ is nearly independent of z and $\vec{M}_e'$ is nearly linear in z for the PDX device is also utilized in the process. In Eq. (9) the n-index matrices are defined by

$$\vec{\vec{n}} = n(z_q)\,\vec{\vec{U}} \tag{10}$$

$$\vec{\vec{n}}_s = \frac{2R}{\mu_0 \Lambda(z_q)}\,\vec{\vec{L}}_{\ell\ell}^{-1}\,(\vec{M}'_\ell \overleftarrow{M}'_\ell) \tag{11}$$

In Eq. (10), $\vec{\vec{U}}$ is the unit matrix and $n(z_q)$ the n-index evaluated at the equilibrium location. Once the loop currents are computed with Eq. (9), the plasma position can be obtained from Eq. (4).

The most unstable eigenvalue of Eq. (9) gives the instability growth rate. The nature of the eigenvalue can be seen easily when there is only one L-circuit. The equation yields an unstable solution when the conditions, $n < 0$ and $n + n_s > 0$, are simultaneously met. The growth rate is given by $-(R_\ell/L_\ell)n/(n + n_s)$, where R_ℓ and L_ℓ are now scalar resistance and inductance of the loop current circuit, respectively. This growth rate is of the same form as the one given by Fukuyama et al. [Eq. (24) of Ref. [13] in the limit of zero plasma mass] for a slightly elongated plasma in a cylindrical shell. The expressions for n_s are, however, different for the two cases. Note that the instability growth time is proportional to the L/R-time of the stabilizing circuit. The proportionality factor, $(n + n_s)/n$, varies, however, from zero to infinity depending upon the magnitude of the 'canonical' n-index [Eq. (10)] and the stabilizing n-index [Eq. (11)]. Thus, the oft-quoted statement that the instability grows with the circuit L/R-time is valid only in a regime in which passive-stabilization effects are small ($|n| \gg n_s$). The expression for the stabilizing n-index [Eq. (11)] embodies simple geometrical effects: plasma motion produces an EMF at the L-circuit proportional to the mutual inductance gradient. This EMF induces an L-current inversely proportional to the L-circuit self-inductance. This current, in turn, produces a radial field at the plasma proportional to the mutual inductance gradient. Hence, the stabilizing n-index is proportional to the factor $(M'_\ell)^2/L_\ell$.

The roles played by a finite plasma resistivity can be investigated most easily when the basic equations are specialized for one L-circuit. Among the E-circuits, only the EF and OH circuits are considered. The plasma current is now allowed to vary and is governed by Eq. (3). The plasma major radius is assumed constant. Neglecting terms of order $M_\ell/L_\ell = O(10^{-3})$, the following equation is obtained:

$$(n + n_s)\,\dot{z} + \left\{\frac{n}{\tau_\ell} + \frac{n}{\tau_e} - \frac{n_s}{\tau_p}\left(1 + \frac{d}{dt}(M_o I_o)/R_p I_p\right)\right\} z = 0 \tag{12}$$

where M_o and I_o are the plasma-OH circuit mutual inductance and OH current, respectively. The characteristic times in this equation are defined by

$$\tau_\ell = \frac{L_\ell}{R_\ell}\,; \quad \tau_e = \frac{I_e}{\dot{I}_e}\,; \quad \tau_p = \frac{L_p}{R_p} \tag{13}$$

Equation (12) shows under what circumstances characteristic times other than the stabilizing circuit L/R-time, τ_ℓ, come into play. The characteristic time for EF current change, τ_e, enters the equation in the same manner as τ_ℓ. However, τ_e is usually much greater than τ_ℓ and can be neglected for the PDX experiments. It is noteworthy that the plasma L/R-time, τ_p, enters the equation differently. It is associated with the stabilizing n-index rather than the canonical n-index. It is further multiplied by a factor, $1 + (d/dt)\,(M_o I_o)/R_p I_p$. This factor is zero when the magnetic flux coupled by the plasma stays constant and hence the Ohmic-flux swing is balanced by the resistive voltage drop. This is the case whenever the plasma major radius and current are held constant. It may be inferred from this conclusion that if the rate of change in the magnetic flux associated with the internal inductance of a finite-size plasma becomes comparable to the resistive drop, a finite contribution from the plasma resistivity may arise. For the PDX experiments, the plasma current is held nearly constant and internal inductance change is negligibly small. Within the framework of the line current theory the plasma resistivity is not expected to be important for the PDX experiments. It should be added here that Jensen [14] found through a more complete MHD analysis that the growth rate of a single-axis tokamak is proportional to the stabilizing-wall resistivity rather than to the plasma resistivity.

3. EXPERIMENTS

3.1. Experimental facilities

Poloidal-field (PF) coil groups are shown in a cross-sectional view of the PDX device (Fig. 1). The PF coil groups considered in this article are the divertor field (DF) coils, equilibrium field (EF) coils for generating equilibrium vertical fields, Ohmic-heating (OH) coils and nulling-field (NF) coils for fine adjustment of the null-field pattern during the discharge initiation. Poloidal fields resulting from the toroidal-field (TF) buss-work (consisting of coil-to-coil transitions, turn-to-turn transitions, and a cancellation loop) must also be considered.

Both the DF coils above the meridian plane and those below are connected in separate series circuits. These two series circuits are then connected in parallel to the DF power supply. The two circuits are also connected to each other at four locations through shorting bars to form a ladder network. An equivalent circuit is shown in Fig. 6. The currents in the top (I_{DFT}) and bottom (I_{DFB}) legs of the DF circuits, as well as the currents in the shorting bars, termed the ladder currents (I_A through I_D), are measured. The currents in DF coils can be divided into the symmetric $[(I_{DFT} + I_{DFB})/2]$ and antisymmetric $[(I_{DFT} - I_{DFB})/2]$ parts. The symmetric part, which produces the divertor configuration, is treated as an external current. The antisymmetric part represents currents circulating in closed paths composed of the top/bottom DF coil pairs and shorting bars. These loop currents, I_1 through I_4, generate a stabilizing radial field. (The loop current, I_0, shown in Fig. 6, flows entirely outside the vacuum vessel and is ignored.) Electrical properties of the loop current circuits are tabulated in Table I. The loop currents and ladder currents are related through simple algebraic relations and the measurements of the ladder currents facilitate determination of the loop currents.

A radial field (RF) amplifier is inserted in series in the I_D shorting bar to provide feedback control of the vertical position. The feedback circuit is schematically shown in Fig. 6. The amplifier is a voltage amplifier and a null output voltage (i.e. effective short circuit) can be maintained by applying zero input signal to the amplifier. In this way, the feedback circuit can be effectively removed from the loop current path without interrupting flow of the stabilizing currents induced by the plasma motion. This feature is utilized for instability growth rate determination. All data are digitized at a 1 ms interval and stored in a computer.

TABLE I. ELECTRICAL PROPERTIES OF THE FOUR LOOP CURRENT CIRCUITS SHOWN IN FIG. 6

	I–1	I–2	I–3	I–4
Self-inductance (mH)	1.65	0.64	0.96	1.68
Resistance (mΩ)	8.8	5.2	7.6	26.8
L/R-time (ms)	187	123	126	63

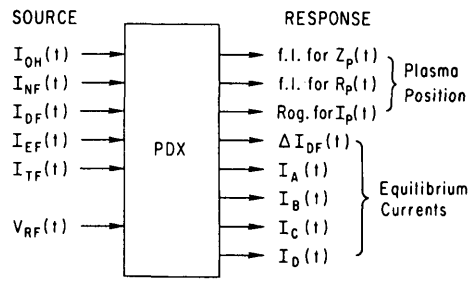

FIG. 7. Six excitation sources and eight responses are considered in constructing transfer functions for the PDX poloidal-coil system.

3.2. Transfer function technique

For determination of both the plasma position and equilibrium loop currents it is necessary to find the response of the PF coil system in the absence of a plasma. This is accomplished using a transfer function technique [15]. We designate by $S_i(t)$ and $S_i(\omega)$ the time-domain excitation of the i-th source and its fast Fourier transform (FFT), respectively. The j-th time-domain response to the i-th excitation and its FFT are similarly designated by $R_{ij}(t)$ and $R_{ij}(\omega)$, respectively. In the absence of a plasma each of the six current and voltage sources is excited individually with a wave form, $S_i^0(t)$, and the j-th response, $R_{ij}^0(t)$, is recorded (Fig. 7). The transfer function between the i-th excitation and j-th response is then defined as

$$H_{ij}(\omega) = \frac{R_{ij}^0(\omega)}{S_i^0(\omega)} \tag{14}$$

In the presence of a plasma all sources are in general excited simultaneously. Their wave forms may also differ from their test shots, $S_i^0(t)$. The 'external' part of the j-th response to this particular combination of the excitations, $R_j^x(t)$, can be obtained from the inverse Fourier transform of the product of the Fourier transformed source functions and appropriate transfer functions,

$$R_j^x(t) = \sum_i \int S_i(\omega)\, H_{ij}(\omega) e^{-i\omega t}\, \frac{d\omega}{2\pi} \tag{15}$$

The response due to the plasma alone is the difference between the total response and the external response.

3.3. Plasma position determination

The plasma radial and vertical position measurements [15] used in this work are unique in two respects: (1) plasma poloidal flux rather than the total flux is determined and compared to an equilibrium MHD theory, and (2) the transfer function technique is used to determine the external flux. The plasma poloidal flux is determined from measurements using a pair of circular flux loops concentric with the plasma ring. The loops used for vertical position measurements are placed at the same major radius and at equidistant locations on either side of the meridian plane (Fig.6). The difference between the flux coupled by the two loops is composed of the external and the plasma contributions. The external contribution, which arises from flux linkage between the flux loops and currents in the coils and eddy currents in the structure, can be subtracted from the total flux by using the transfer function technique. The remaining plasma flux is related to the vertical plasma displacement. The experimentally determined plasma flux is then compared with theoretical calculations to determine the vertical position of the magnetic axis of the plasma. The radial position is determined in a similar manner by using two groups of flux loops located at two different major radial positions. The theoretical poloidal flux linked by a flux loop is calculated after equilibrium flux surfaces are obtained by the PEST code for a given set of plasma and coil currents. The plasma position determined in this way is shown in Fig. 8 for a discharge typical for the growth rate measurement experiments. Figure 8a shows the vertical position (ordinate) against time (abscissa), and Fig. 8b the radial position (abscissa) versus time (ordinate). Figure 8c is the composite vertical (ordinate) and radial (abscissa) position diagram with time as a parameter.

Measurements of the instability growth rates are made by utilizing both the vertical and radial feedback controls. A plasma of desired properties is first produced in the stable region [point A in Fig. 8c] and then radially moved into an unstable region (point B) while holding the vertical position unchanged. At the desired radial position, vertical feedback control is removed, and radial feedback maintains position unchanged allowing the plasma to drift upward or downward at a constant radius (point C). The plasma is then brought back into the stable region (point D) for controlled discharge termination. Note that the stabilizing loop current through the RF amplifier induced by the plasma motion is not impeded during the growth rate measurement because the removal of

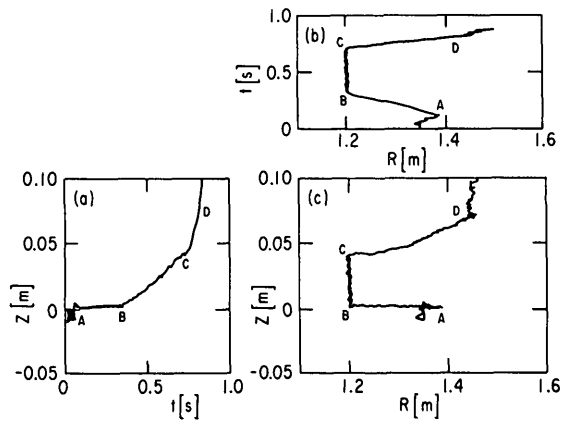

FIG.8. Radial and vertical positions of magnetic axis of plasma. (a) vertical position (ordinate) versus time; (b) radial position (abscissa) versus time; (c) composite diagram of vertical position (ordinate) versus radial position (abscissa) with time as parameter.

the vertical position feedback is accomplished not by shutting off the amplifier but by maintaining a zero input voltage.

It is seen in Fig. 8c that the vertical position can be held constant as the plasma is radially moved into an unstable region, demonstrating that the vertical-position feedback-control system using an amplifier with a modest power (100 kW) rating, aided by passive stabilization, is sufficient to control the instability completely up to an n-index value of -1.5. The plasma current ranged from 170 to 310 kA in these experiments.

3.4. Radial field error

The equilibrium location defined by Eq. (8) is the position where a filamentary plasma carrying a negligible current can remain stationary having been placed there carefully. Had such a plasma been placed at a point away from the equilibrium point within the stable region and had its major radius been held constant, it would have moved toward the equilibrium point at that radius. If placed in an unstable region, the plasma would move away from the equilibrium point. The rate at which this motion takes place must, in either case, be measured from the equilibrium point. It should be noted that the equilibrium point may also be changing with time. For a tokamak with a perfect vertical symmetry the equilibrium plasma location lies on the structural meridian plane. In this case the vertical instability growth rate can be determined from a logarithmic plot of the plasma position

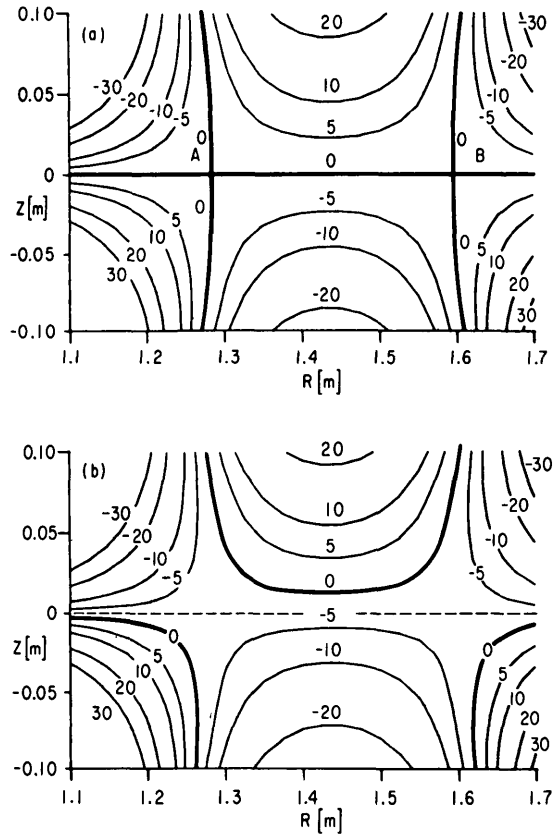

FIG. 9. Contour plot of radial field (a) with perfect symmetry, and (b) with asymmetric TF busswork currents. Zero radial field contours (bold lines) show large distortions near saddle points (A and B) in presence of TF busswork current. This has significant effects on interpretation of instability growth rate data.

measured from the meridian. Any deviation of the equilibrium location from the meridian would enter as an additive (rather than inconsequential multiplicative) term in the logarithmic position function and would result in an error in the growth rate determination. Such errors must be corrected for when a small growth rate is to be measured.

In PDX there are two sources of radial field error that cause deviation of the equilibrium location. The first of these arises from the presence of a TF busswork which is not located symmetrically with respect to the meridian plane. The error caused by this asymmetry is nearly constant in time but is space-dependent. The second source of error are the L-currents driven due to small coupling between the E-circuits and the L-circuits. This coupling arises from imperfect symmetry of the PDX device. The resultant radial error field is relatively uniform in space but is time-varying.

A contour plot of the radial field is shown in Fig. 9a calculated for typical values of DF, EF, and OH currents assuming a perfect symmetry of these coils with respect to the structural meridian plane. Contours of zero radial field are shown in bold lines. Two intersections of these lines are saddle points of the contour map, and their radial locations represent the boundaries between the stable and unstable regions. The zero-field lines are the contours of vertical equilibrium positions. Addition of the asymmetric field produced by the TF busswork current distorts the equilibrium contours as shown in Fig. 9b. Because of shallow vertical gradient of the radial field near the saddle points, additional asymmetric field of only a few gauss can shift the equilibrium location significantly. Reliable determination of the growth rate in the regions of small n-index is impossible without correcting for this error.

The time-varying radial error field can be corrected for if the equilibrium currents introduced in Section 2.2 can be calculated. The equilibrium currents are theoretically calculable from Eq. (7). The inductance matrix, $\vec{\vec{L}}_{\ell e}$, is, however, in general unknown: all elements would be zero were the system ideally symmetric. Instead of solving the equations we obtain the equilibrium currents by using the transfer function technique, each of the six external sources, OH, NF, DF, EF and TF, and the RF amplifier, is individually excited, and the L-currents in the absence of a plasma are measured to construct transfer functions. The equilibrium currents for an actual plasma shot can be obtained from Eq. (15). This correction for the time-varying equilibrium position is possible only because the stabilizing currents in PDX flow in well-defined paths and can be experimentally measured.

3.5. Experimental growth rate

In analysing data such as those shown in Fig. 8, the equilibrium vertical location corresponding to the radial position of the plasma is determined for each instance of time. First, the equilibrium loop currents are determined using the transfer functions. Then the equilibrium location is determined from Eq. (8) using the measured E-currents. The TF busswork appears through an element of the mutual inductance array, $\vec{M}'_e$. A typical logarithmic plot of the vertical plasma position (measured from the equilibrium location) against time is shown in Fig. 10. The slope of the least-square fit (solid line) gives the vertical instability growth rate.

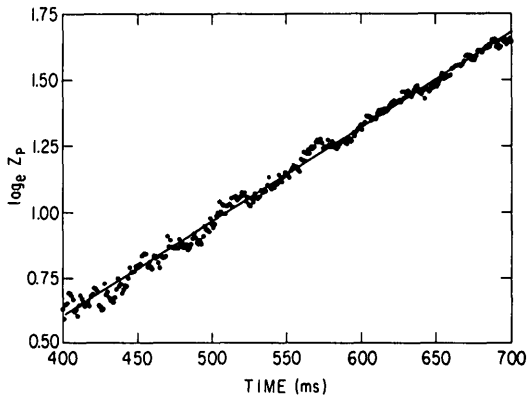

FIG.10. Logarithmic plot of vertical position against time for an unstable case. Solid line is least-square fit to data taken every millisecond.

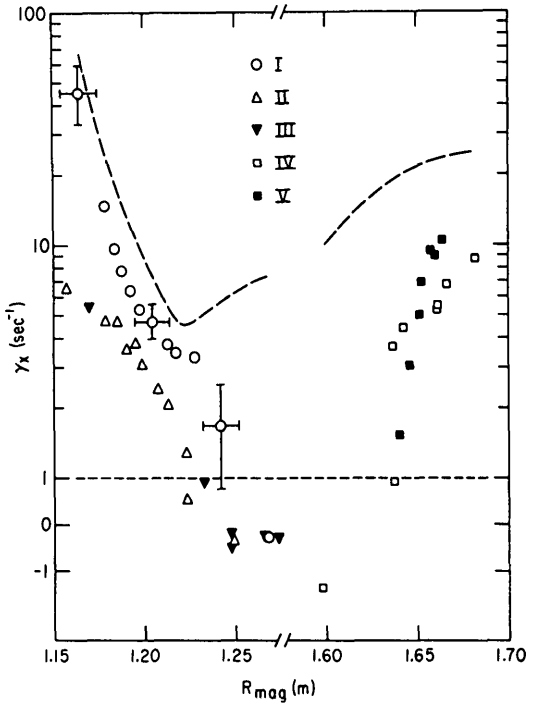

FIG.11. Experimentally determined vertical instability growth rate plotted against magnetic axis location for five groups of data. Groups I–III are for inner unstable region (standard-D) and groups IV–V for outer unstable region (inverted-D). See Table II for parameter ranges. Ordinate is a composite logarithmic/linear scale. Part of stable region is omitted from abscissa.

The experimentally determined growth rate is plotted in Fig. 11 against the magnetic axis location for five groups of data. The first three groups (I–III) are for the inner unstable region and the last two (IV–V) for the outer unstable region. Different groups are obtained either for different plasma currents or for different experimental occasions. Ranges of some discharge parameters are summarized in Table II for these groups. Estimated error bars are indicated in the figure for typical shots in the low-, mid- and high-growth rate regimes. The measured growth time approaches in some cases the plasma L/R-time shown in the table. No clear correlation is found in PDX, however, between the instability growth time and plasma L/R-time, in agreement with the discussion of Section 2.2. The dotted curves in Fig.11 indicate approximate values which would have been obtained had no corrections against radial field error been included. Such corrections are clearly essential for the determination of small growth rate, but they are less important for faster growth rate.

TABLE II. RANGE OF PLASMA PROPERTIES FOR THE FIVE EXPERIMENTAL DATA GROUPS

R_p, I_p, V_L and L_p are major radius, current, one-turn voltage and self-inductance, respectively. The ratios V_L/I_p and L_pI_p/V_L are average resistance and L/R-time, respectively.

Group	I	II	III	IV	V
R_p(cm)	116.5~126.6	115.7~124.9	117.0~127.2	159.7~168.2	164.0~166.4
I_p(kA)	217~225	282~301	299~312	171~203	178~235
V_L(V)	0.5~1.0	0.8~1.0	1.1~1.3	1.1~1.4	1.4~1.7
L_p(μH)	3.1	3.1	3.1	4.8	4.8
V_L/I_p($\mu\Omega$)	2.8~4.8	2.8~3.3	3.7~4.2	5.7~7.9	5.5~8.9
L_pI_p/V_L(s)	0.7~1.1	0.9~1.1	0.7~0.8	0.6~0.8	0.5~0.9

4. COMPARISON OF EXPERIMENTS AND THEORY

A theory that can model the PDX experiments well would have to account for the response of plasma current distribution to stabilizing loop currents induced by the plasma motion in a self-consistent manner. Such a resistive theoretical formalism may exist [16], but its free-boundary computational counterpart for the PDX configuration is not available at this time. Instead of attempting to find out how accurately such a theory agrees with the experiments, we present the experimental data in terms of some dimensionless parameters and compare them with predictions of simple theories. While the physical models used in these theories are not sophisticated enough to fully represent the experimental situation, their analytical simplicity permits greater physical insight into the phenomena under study.

4.1. Growth rate in terms of n-index and line current theory

In Fig. 12, the experimental growth rates are plotted against the magnetic-field decay index (n-index). Note that the highest growth rate point is plotted against a different ordinate. (This will also be true for Figs 13 and 14.) The n-index value at the magnetic axis location is computed for each discharge using coil currents averaged over the same period over which the growth rate is determined. Transition from the stable to unstable configuration takes place almost exactly at n = 0 as predicted by simple theories. This indicates that higher-order stabilizing features of the plasma shape [17, 18], e.g. rectangularity, are small under the present experimental conditions. In the range $-0.8 < n < 0$, the growth rate is almost solely dependent on the n-index at the magnetic axis. The growth

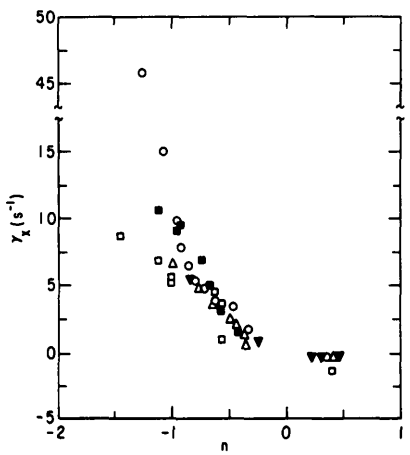

FIG.12. Experimental growth rate plotted against value of n-index on magnetic axis. See Fig.11 for symbol definitions and Table II for parameter ranges.

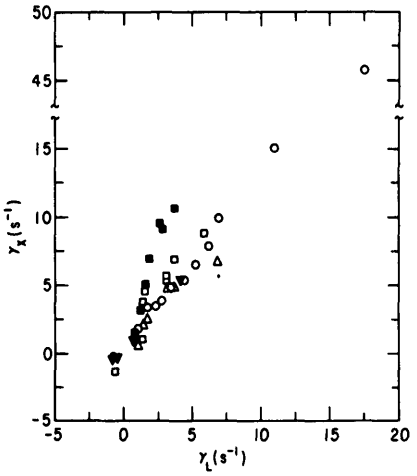

FIG.13. Experimental growth rate plotted against theoretical growth rate based upon line current model. See Fig.11 for symbol definitions and Table II for parameter ranges.

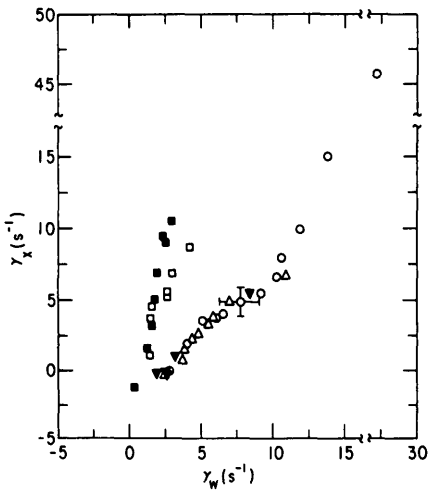

FIG.14. Experimental growth rate plotted against Wesson's growth rate. See Fig.11 for symbol definitions and Table II for parameter ranges. Wesson's theory is based upon cylindrical, elliptically elongated plasma surrounded by confocal resistive wall. Clearly different trends of standard-D and inverted-D groups suggest influence of toroidal effects, most notably plasma triangularity.

TABLE III. RANGE OF NORMALIZED FOURIER EXPANSION COEFFICIENTS OF THE OUTERMOST MAGNETIC SURFACE (Eq.(1)) FOR THE FIVE EXPERIMENTAL DATA GROUPS

a_2, a_3 and a_4 are ellipticity, triangularity and rectangularity, respectively. $\epsilon\beta_p$ is the product of the inverse aspect ratio and the ratio of the kinetic to poloidal magnetic pressures.

	I	II	III	IV	V
$a_2 \times 10^2$	$-5.3 \sim -12.4$	$-5.8 \sim -10.7$	$-4.7 \sim -9.9$	$-1.2 \sim -6.3$	$-3.4 \sim -5.2$
$a_3 \times 10^2$	$+6.6 \sim +8.3$	$+6.4 \sim +7.3$	$+6.1 \sim +7.2$	$-4.8 \sim -6.4$	$-5.4 \sim -6.3$
$a_4 \times 10^2$	$-0.3 \sim -2.8$	$-0.4 \sim -2.4$	$-0.7 \sim -2.8$	$-1.8 \sim -3.7$	$-2.3 \sim -2.6$
$\epsilon\beta_p \times 10^2$	$6.9 \sim 8.4$	$3.8 \sim 4.4$	$3.6 \sim 4.4$	$6.4 \sim 8.6$	$4.8 \sim 7.0$

rate becomes widely scattered, however, in the range $n < -1$, for a given value of n, as the plasma shape becomes increasingly non-circular.

The experimental growth rate is compared in Fig.13 with the rate predicted by the line current theory [the most unstable eigenvalue of Eq. (9)]. Two trends are evident. First, the experimental growth rate of the standard-D (Group I–III) plasma follows the line current theory predictions well in the small-growth-rate ($<15\ s^{-1}$) regime. The slope of a best-fit line through the standard-D data except for the highest-growth-rate point is 1.7. In a high-growth-rate regime, however, the deviation from the theory is significant. Second, the inverted-D (Group III–IV) plasmas appear to follow a line considerably steeper than the standard-D plasmas. These disagreements again indicate the inadequacy of the line current theory.

4.2. Growth rate in terms of ellipticity

In theories of vertical instability, it is a common practice to relate the instability growth rate to some parameters which characterize the shape of magnetic surfaces. We attempt in this section to use such shape parameters described earlier (Section 2.1) to correlate the measured growth rates. Using the measured time-averaged coil currents, plasma current and magnetic axis location, a MHD equilibrium is obtained by the PEST computer code for each discharge, and the shape parameters are computed in accordance with Eq. (1). Ranges of some of these parameters are tabulated in Table III for the five groups of data.

Analytical theories using a simple physical model were developed by Wesson [3] and also by Fukuyama et al. [13]. Wesson treated in a cylindrical approximation a vertically elongated, elliptical plasma within a confocal resistive wall. In the limit of a large wall L/R-time in comparison with the Alfvén transit time, his result (second equation in the left-hand column, p. 119, Ref. [3]) can be written as

$$\gamma_w = \frac{(R_w/R_p)^2 e}{\tau_w\{1 - (R_w/R_p)^2 e\}} \qquad (16)$$

where (R_w/R_p) is the ratio of the wall radius to the plasma radius and τ_w the wall L/R-time. The ellipticity in a conventional definition is designated by $e = (b-a)/(b+a)$, where a and b are the horizontal and vertical semi-axes of the plasma, respectively. This result states that the product of the growth rate and the wall L/R-time is a function of a single dimensionless parameter, $(R_w/R_p)^2 e$. The PDX experimental situations are different from the simple physical model used by Wesson in three important respects: (1) the plasma is toroidal rather than cylindrical, (2) stabilization is provided by a discrete coil system rather than a confocal resistive wall, and (3) the plasma current distribution is not uniform. Nevertheless, comparison with his theory is inviting because of its analytical transparency.

In Fig. 14, the experimental growth rate is plotted against the right-hand side of Eq. (16). The coefficient, $\tilde{a}_0$, of the plasma shape parameter expansion [Eq.(1)] is used for R_p. The radius of an equivalent resistive wall is arbitrarily taken to be 0.7 m, approximately the location of the loop (DF) current coils (see Fig. 1). The resistive wall L/R-time is taken to be 0.13 s, comparable to the actual L/R-times of the loop current

circuits (see Table I). The negative of a_2 defined following Eq. (1) is used for e.

The difference between the standard-D and inverted-D configurations is now more evident than in Fig. 13. The standard-D data, except for the highest-growth-rate point, can be fitted by a line with approximately unity slope. The inverted-D data follow a line with a three times greater slope. When different values are chosen for R_w and τ_w, the slopes of these lines change. But the clear distinction between the two groups remains. This observation is in contrast to a conclusion from the Tokapole experiments [8] in which both the configurations exhibited similar stability characteristics. The most prominent difference between the shapes of the standard-D and inverted-D configurations is the sign of their triangularity parameter: the former has a positive triangularity and the latter negative (see Fig. 5). Thus, the triangular deformation of the plasma with a negative triangularity appears to enhance the instability of an elliptically elongated plasma, while the deformation with a positive triangularity tends to stabilize the instability.

4.3. Triangularity corrections

There appear to be no analytically tractable theories on the passively stabilized vertical instability which include toroidal effects such as a triangular deformation of the plasma. A theory by Yamazaki et al. gives an analytical expression (Eq. (30) of Ref. [10]) for the growth rate as an expansion in the shape parameters defined in Eq. (1). The theory is based upon a perfectly conducting (rather than resistive) wall and is, therefore, not directly applicable to the PDX experiments. The form with which these shape parameters enter into the growth rate expression is of interest, however. According to the theory, terms involving the ellipticity (a_2) and triangularity (a_3) are grouped as

$$-8a_2 - \frac{113}{6}(\epsilon\beta_p)a_3 \qquad (17)$$

where ϵ is the inverse aspect ratio and β_p the ratio of the kinetic to poloidal magnetic pressures. The vertical elongation ($a_2 < 0$) corresponds to destabilization. Negative triangularity is destabilizing and the positive triangularity is stabilizing, according to this theory. This conclusion is in qualitative agreement with the experimental observations discussed in the previous section. The ratio of triangularity to ellipticity contributions is $113/48(\epsilon\beta_p)a_3/a_2$, according to this theory.

Wesson's theory gives the growth rate for a purely elliptically elongated plasma. If a triangularity correction of the form

$$\gamma = \gamma_w - \frac{C}{\tau_w}(\epsilon\beta_p)(a_3 - a_3^0) \qquad (18)$$

is added to this growth rate, the standard-D and inverted-D groups can now be represented roughly by a single curve in a plot of the experimental and theoretical growth rates in the manner of Fig. 14. In Eq. (18), $C \approx 70$ is a dimensionless coefficient adjusted to obtain a reasonable fit. A displacement of the 'origin' of the triangularity by an amount $a_3^0 \approx 0.03$ appears to be needed to obtain such a representation. For small values of ellipticity, $(R_w/R_p)^2 e \ll 1$, the ratio of triangularity to ellipticity contributions is $C(R_p/R_w)^2(\epsilon\beta_p)(a_3 - a_3^0)/a_2$. The numerical factor, $C(R_p/R_w)^2 \approx 13$, is greater than the theoretical value, $113/48 = 2.4$, by a factor of approximately five. The difference may have arisen because the physical model used in the theory is not directly applicable to the experimental situation, or because the theory uses a small parameter expansion.

5. CONCLUSIONS

The strength of vertical instability of a diverted plasma is determined experimentally in the PDX device for a range of the n-index value, $-1.5 < n < +0.5$, in both the standard-D and inverted-D configurations. In PDX, stabilizing currents are induced mostly in the divertor coils connected in a parallel ladder network and flow in well-defined paths. This is one feature that distinguishes the present experiments from previously reported results in which some or all of the stabilizing currents flowed in less clearly defined paths in the surrounding walls. This feature allows determination of the equilibrium loop currents and calculations of the radial error field corrections which are essential to accurate measurements of small instability growth rates. For this reason, the PDX device is well suited for measurements of the instability strength and for testing the efficacy of stabilization by means of a discrete coil system. It is shown experimentally that the discrete coil system used in PDX is effective in partially stabilizing the vertical instability. It is shown further that the instability can be completely controlled up to an n-index value of -1.5 by an additional active feedback system employing a moderate-power

(100 kW) amplifier when the plasma current is in the range 170–310 kA. These instability studies extend from a stable regime to an unstable regime with growth rate up to 45 s^{-1}. No clear correlation is found in PDX between the measured growth time and the plasma L/R-time in line with theoretical expectations. The measured growth time ranges from 10^4 to 10^6 times the Alfvén transit time. This is one to four orders of magnitude greater than previously reported results and is close to values expected in fusion reactors.

The measured growth rate can reasonably be represented by the n-index alone up to its value of −0.8, but the growth rate scatters widely for a given value of the n-index for $n < -1.0$. Transition from the stable to unstable regimes occurs almost exactly at $n = 0$. This suggests that any stabilizing effects, such as rectangular deformation of the plasma [17, 18], are small under conditions encountered in the present experiments. The line current theory is shown to be capable of predicting the growth rate reasonably well when it is less than about 15 s^{-1}, but the theory gives growth rates too small when they are greater than this value. Furthermore, the theory fails to predict evidently different behaviours of the standard-D and inverted-D configurations.

A way to characterize the shape of a poloidal flux surface systematically in terms of a Fourier expansion [Eq. (1)] is devised. The first term of the expansion is an equivalent plasma minor radius. The following three non-zero terms represent the ellipticity, triangularity, and rectangularity. The experimental growth rates are correlated to one or more of these dimensionless shape parameters using results of analytical theories. Comparisons with Wesson's theory [3] based upon a cylindrical, elliptically elongated plasma surrounded by a confocal resistive wall show that the inverted-D configuration is approximately three times more unstable than the standard-D configuration for the same ellipticity. This difference between the two data groups is attributed to a triangular deformation of the plasma. The inverted-D configuration is further destabilized compared to a purely elliptical deformation because of its negative triangularity and the standard-D is stabilized by its positive triangularity. This interpretation is in qualitative agreement with an analytical theory by Yamazaki et al. [10]. The amount of triangularity correction, needed to bring both the inverted-D and standard-D configurations into a single group, is estimated. The magnitude of the triangularity contribution relative to the ellipticity contribution appears to be greater in the experiments than in the theory by approximately a factor of five. However, the physical model used in the theory is based upon a perfectly conducting wall and is not representative of the PDX device. More accurate assessment of the toroidal effects must await a better applicable theory.

ACKNOWLEDGEMENTS

The authors wish to thank the PDX operating crew for its assistance in conducting the experiments. This work was performed under the United States Department of Energy Contract No. DE-AC02-76-CH03073.

REFERENCES

[1] See, e.g. "International Tokamak Reactor: Zero Phase", IAEA, Vienna (1980).
[2] OKABAYASHI, M., MAEDA, H., TAKAHASHI, H., REUSCH, M., Nucl. Fusion **21** (1981) 271.
[3] WESSON, J.A., Nucl. Fusion **18** (1978) 87.
[4] REBHAN, E., SALAT, A., Nucl. Fusion **18** (1978) 1431.
[5] MEADE, D., ARUNASALAM, V., BARNES, C., BELL, M., BITTER, M., et al., in Plasma Physics and Controlled Nuclear Fusion Research (Proc. 8th Int. Conf. Brussels, 1980) Vol.1, IAEA, Vienna (1981) 665.
[6] BORTNIKOV, A.V., BREVNOV, N.N., GUSS, W.C., GERASIMOV, S.N., ZHUKOVSKI, V.G., KUZNETSOV, N.V., PERGAMENT, V.I., HUTCHINSON, D.P., KHIMCHENKO, L.N., Sov. J. Plasma Phys. **4** (1978) 144.
[7] CIMA, G., ROBINSON, D.C., THOMAS, C.L., WOOTTON, A.J., in Plasma Physics and Controlled Nuclear Fusion Research (Proc. 6th Int. Conf. Berchtesgaden, 1976) Vol. 1, IAEA (Vienna) (1977) 335.
[8] LIPSCHULTZ, B., PRAGER, S.C., TODD, A.M.M., DeLUCIA, J., Nucl. Fusion **20** (1980) 683.
[9] TAKAHASHI, H., BOL, K., FISHMAN, H., MAEDA, H., OKABAYASHI, M., REUSCH, M., Paper 5 p12, Bull. Am. Phys. Soc. **25** (1980) 928.
[10] YAMAZAKI, K., FISHMAN, H. TODD, A.M.M., OKABAYASHI, M., Axisymmetric Stability of Vertically Asymmetric Tokamaks at Large Beta Poloidal, Princeton Plasma Physics Lab. Rep. PPPL-1831 (1981).
[11] JOHNSON, J.L., DALHED, H.E., GREEN, J.M., GRIMM, R.C., HSIEH, Y.Y., JARDIN, S.C., MANICKAM, J., OKABAYASHI, M., STORER, R.G., TODD, A.M.M., VOSS, D.E., WEIMER, K.E., J. Comput. Phys. **32** (1979) 212.
[12] REBHAN, E., SALAT, A., Nucl. Fusion **16** (1976) 805.
[13] FUKUYAMA, A., SEKI, S., MOMOTA, H., ITATANI, R., Jpn. J. Appl. Phys. **14** (1975) 871.
[14] JENSEN, T.H., J. Plasma Phys. **26** (1981) 351.
[15] REUSCH, M., OKABAYASHI, M., OWENS, D.K., SCHMIDT, G.L., TAKAHASHI, H., Paper 5 p11, Bull. Am. Phys. Soc. **25** (1980) 927.

[16] JENSEN, T.H., THOMPSON, W.B., J. Plasma Phys. **19** (1978) 227; JENSEN, T.H., McCLAIN, F.W., J. Plasma Phys. **20** (1978) 61; McCLAIN, F.W., JENSEN, T.H., J. Plasma Phys. **26** (1981) 431.

[17] SHEFFIELD, G.V., Vertical Stability of Tokamak-Type Equilibria as a Function of Cross-Sectional Shape, Princeton Plasma Physics Lab. Rep., MATT-999 (1973).

[18] LACKNER, K., MacMAHON, A.B., Nucl. Fusion **14** (1974) 575.

(Manuscript received 15 June 1982
Final manuscript received 19 October 1982)